

In situ Qubit Frequency Tuning Circuit for Scalable Superconducting Quantum Computing: Scheme and Experiment

Lei Jiang^{1,2,*}, Yu Xu^{2,3,*}, Shaowei Li^{2,3,*}, Zhiguang Yan^{1,2,†}, Ming Gong^{1,2,3}, Tao Rong^{1,2}, Chenyin Sun^{1,2}, Tianzuo Sun^{1,2}, Tao Jiang^{1,2}, Hui Deng^{1,2,3}, Chen Zha^{2,3}, Jin Lin^{2,3}, Fusheng Chen^{2,3}, Qingling Zhu^{2,3}, Yangsen Ye^{1,2}, Hao Rong^{1,2}, Kai Yan^{2,3}, Sirui Cao^{1,2}, Yuan Li^{1,2}, Shaojun Guo^{1,2}, Haoran Qian^{1,2}, Yisen Hu^{1,2}, Yulin Wu^{1,2}, Yuhuai Li^{1,2,3}, Gang Wu^{1,2,3,4}, Xueshen Wang^{5,3}, Shijian Wang⁵, Wenhui Cao^{5,3}, Yeru Wang⁶, Jinjin Li^{5,3,‡}, Cheng-Zhi Peng^{1,2,3}, Xiaobo Zhu^{1,2,3,6,§}, and Jian-Wei Pan^{1,2,3,¶}

¹Hefei National Research Center for Physical Sciences at the Microscale and School of Physical Sciences, University of Science and Technology of China, Hefei 230026, China

²Shanghai Research Center for Quantum Science and CAS Center for Excellence in Quantum Information and Quantum Physics, University of Science and Technology of China, Shanghai 201315, China

³Hefei National Laboratory, University of Science and Technology of China, Hefei 230088, China

⁴University of Science and Technology of China, Shanghai Research Institute, Shanghai 201315, China

⁵National Institute of Metrology, Beijing 102200, China and

⁶Jinan Institute of Quantum Technology, Jinan 250101, China

(Dated: August 1, 2024)

Frequency tunable qubit plays a significant role for scalable superconducting quantum processors. The state-of-the-art room-temperature electronics for tuning qubit frequency suffers from unscalable limit, such as heating problem, linear growth of control cables, etc. Here we propose a scalable scheme to tune the qubit frequency by using *in situ* superconducting circuit, which is based on radio frequency superconducting quantum interference device (rf-SQUID). We demonstrate both theoretically and experimentally that the qubit frequency could be modulated by inputting several single pulses into rf-SQUID. Compared with the traditional scheme, our scheme not only solves the heating problem, but also provides the potential to exponentially reduce the number of cables inside the dilute refrigerator and the room-temperature electronics resource for tuning qubit frequency, which is achieved by a time-division-multiplex (TDM) scheme combining rf-SQUID with switch arrays. With such TDM scheme, the number of cables could be reduced from the usual $\sim 3n$ to $\sim \log_2(3n) + 1$ for two-dimensional quantum processors comprising n qubits and $\sim 2n$ couplers. Our work paves the way for large-scale control of superconducting quantum processor.

INTRODUCTION

Recent years quantum advantage has been realized on superconducting quantum computing system built upon frequency tunable superconducting qubit[1–4], due to its remarkable flexibility of fulfilling various quantum gates with high fidelity [5–8], controlling the coupling strength between qubits when serving as couplers [6, 9], etc. Currently, tuning the transition frequency of frequency tunable qubit i.e., Z-control is achieved by inputting a constant direct current (DC) signal or a long-time pulsed square wave microwave signal from room-temperature electronics into the low temperature qubit chip. However, this scheme suffers from the heating problem caused by consumed energy on the attenuators along the coaxial cables within the dilute refrigerator[1, 2]. And the number of Z-control line increases linearly with number of qubits and couplers, challenging the limited inner space of the dilute refrigerator when scaling up to thousands of qubits. These factors contribute to the bottleneck of the scalability of superconducting quantum processors.

Here we propose a scalable scheme to tune the qubit frequency by *in situ* superconducting loop based on radio frequency superconducting quantum interference device

(rf-SQUID). Today rf-SQUID is prevalently used as magnetic flux and field sensor to detect the external magnetic field [10, 11]. And applying rf-SQUID to generate magnetic flux has also been investigated since 1970s [12–14]. There are also many works applying rf-SQUID to superconducting quantum computing e.g., rf-SQUID directly acting as qubit [15–17], using rf-SQUID to detect quantum states of qubits [18, 19], rf-SQUID acting as tunable coupler [20, 21], etc. However, applying rf-SQUID to control qubit frequency in a scalable way has rarely been reported.

In this paper, we propose a scalable scheme to control qubit frequency by utilizing rf-SQUID as a magnetic flux generator. In our scheme an rf-SQUID is designed around a qubit to provide qubit with magnetic flux via mutual inductance. We will demonstrate both theoretically and experimentally that the state of rf-SQUID i.e., superconducting current inside rf-SQUID could be modulated by a pulsed signal. The state of rf-SQUID will stay the same after modulation indefinitely due to the thermal excitation rate approaching zero [22], thus providing qubits with constant magnetic flux to keep qubit frequency stable. In experiment, we also compare the stability of qubit frequency obtained in classical room-temperature elec-

tronics scheme and the rf-SQUID scheme. The relative standard deviation (RSD) of magnetic flux fluctuation provided for qubit under rf-SQUID scheme is 24.5 parts per million (PPM), outperforming 55.0 PPM observed under room-temperature electronics scheme (driven by 16-bit resolution digital-to-analog converter[2]). Compared with the classical Z-control scheme based on room-temperature electronics, our scheme not only requires several single, short-duration pulsed signals input to tune qubit frequency, which could overcome the heating problem rising from the continuous signal input, but also could further reduce the room-temperature electronics resource for Z-control and the number of Z-control cables in dilute refrigerator from usual $\sim 3n$ to $\sim \log_2(3n) + 1$ for quantum processor with n qubits and $\sim 2n$ couplers, so as to move forward to low-power and scalable control of large-scale superconducting quantum processors.

THE MODEL AND SCHEME

Fig. 1(a) shows the circuit diagram of our scheme. There is an rf-SQUID (red) locating around qubit (green) which interacts with qubit through mutual inductance M_{23} . To modulate the state of rf-SQUID, we design a transmission line named rf-bias line (blue) around rf-SQUID which not only interacts with rf-SQUID by mutual inductance M_{12} but also directly interacts with qubit through mutual inductance M_{13} . In this way, rf-bias line also works as the microwave drive line (XY-line) for qubit. A single square wave pulse is input into rf-bias line to modulate the state of rf-SQUID i.e., the superconducting current inside the loop of rf-SQUID. After modulation the superconducting current inside rf-SQUID provides qubit with magnetic flux through M_{23} , which tunes the qubit frequency.

In this scheme, we focus on the rf-SQUID with hysteresis parameter (screening parameter) $\beta_e = 2\pi \frac{I_c L}{\Phi_0} > 1$, where I_c is the critical Josephson current of the Josephson junction (JJ) in rf-SQUID, L is the self-inductance of the superconducting loop and $\Phi_0 = h/2e \approx 2.07 \text{ mV} \cdot \text{ps}$ is the magnetic flux quantum. When $\beta_e > 1$, the potential energy of rf-SQUID will exhibit many local potential wells (metastable states) as shown in Fig 1(c) and the local potential wells Φ_m has the approximation $\Phi_m \approx n\Phi_0$ with $n = 0, \pm 1, \pm 2, \dots, \pm \lfloor \beta_e/2\pi + 1/4 \rfloor$ (see Eq. 2). Moreover, the relationship between the external magnetic flux Φ_e and the total magnetic flux Φ of rf-SQUID will exhibit hysteresis as shown in Fig. 1(d), which is indicated by Eq.1. In this case, the rf-SQUID is referred to as hysteretic [11, 23, 24]. Since $\Phi = \Phi_e + IL$, the total magnetic flux Φ of rf-SQUID i.e., the state of rf-SQUID determines the superconducting current I inside rf-SQUID for $\Phi_e = 0$.

$$\frac{\Phi_e}{\Phi_0} = \frac{\Phi}{\Phi_0} + \frac{\beta_e}{2\pi} \sin\left(2\pi \frac{\Phi}{\Phi_0}\right) \quad (1)$$

$$\begin{aligned} \Phi_{e,c} &= [n \pm (\beta_e/2\pi + 1/4)]\Phi_0 \\ \Phi_m &\approx n\Phi_0 \\ n &= 0, \pm 1, \pm 2, \dots, \pm \lfloor \beta_e/2\pi + 1/4 \rfloor \end{aligned} \quad (2)$$

The state of rf-SQUID could be modulated by a pulsed signal. The dynamical differential equation rises from the resistive-capacitive shunted Josephson junction (RSCJ) model of rf-SQUID (see Fig 1(a)) [11, 23, 24]

$$\begin{aligned} \frac{d^2(\Phi/\Phi_0)}{dt^2} &= -\frac{\beta}{\sqrt{LC}} \frac{d(\Phi/\Phi_0)}{dt} - \frac{\beta_e}{2\pi} \frac{1}{LC} \sin\left(2\pi \frac{\Phi}{\Phi_0}\right) \\ &+ \frac{1}{LC} \left(\frac{\Phi_e(t) - \Phi}{\Phi_0} \right) \end{aligned} \quad (3)$$

where C is the shunted capacitance of the JJ, R is the shunted resistance of the JJ, L is the self-inductance of the loop and $\beta = \frac{1}{R} \sqrt{\frac{L}{C}}$ is the quality factor of rf-SQUID. With the help of Eq. 3, it's straightforward to deduce the dynamical response of rf-SQUID to a pulsed external magnetic flux $\Phi_e(t)$ when $\beta/\beta_c > 1$ (overdamped condition), $\beta/\beta_c = 1$ (critical damped condition) or $\beta/\beta_c < 1$ (underdamped condition) where $\beta_c = 2.97\sqrt{\beta_e/2\pi}$, as shown in Fig. 1(e) [12, 23, 24]. These dynamical results could be illustrated by a physical picture that a particle with mass C slips down a tilted washboard potential once the local potential barrier vanishes when the input magnetic flux signal exceeds the threshold value $\Phi_{e,c}$ (see Eq. 2 deriving from Eq. 1). And the final stop position is related with the damping condition β/β_c . Additionally, the final state of rf-SQUID varies linearly with the amplitude of input magnetic flux once the amplitude exceeds the thresholds regardless of the damping conditions, which is shown in Fig. 1(f). This linear magnetic flux transition relationship is crucial to modulate rf-SQUID to reach any desired local potential well. All these dynamical properties inspire us the scheme of modulating rf-SQUID by a pulsed signal.

For $\beta/\beta_c \geq 1$ (overdamped or critical damped condition), the amplitude of the input pulse should be chosen near the threshold value indicated by the target position. To be specific, let's suppose the initial state of rf-SQUID is $\Phi_i \approx n_i\Phi_0$, $n_i > 0$ and the target final state is $\Phi_f \approx n_f\Phi_0$ with $n_f > n_i$. In this case, the pulse amplitude must satisfy $\Phi_e/\Phi_0 \in [n_f - 1 + (\beta_e/2\pi + 1/4), n_f + (\beta_e/2\pi + 1/4)]$ and vice versa for other $n_i, n_f < 0$ cases. Only a single pulse input is needed in principle.

For $\beta/\beta_c < 1$ (underdamped condition), it's usually hard to modulate rf-SQUID to a specific position by inputting a single pulse due to the multiple magnetic flux transition phenomenon (see Fig. 1(e)) [12, 23]. However, it's still able to modulate rf-SQUID to a target position by inputting several single pulses. For example, let's suppose that in this case, the basic magnetic flux transition $\Delta\Phi$ satisfies $\Delta\Phi > 0$. Firstly, inputting a single pulse with negative amplitude $\Phi_{e,1}/\Phi_0 \in$

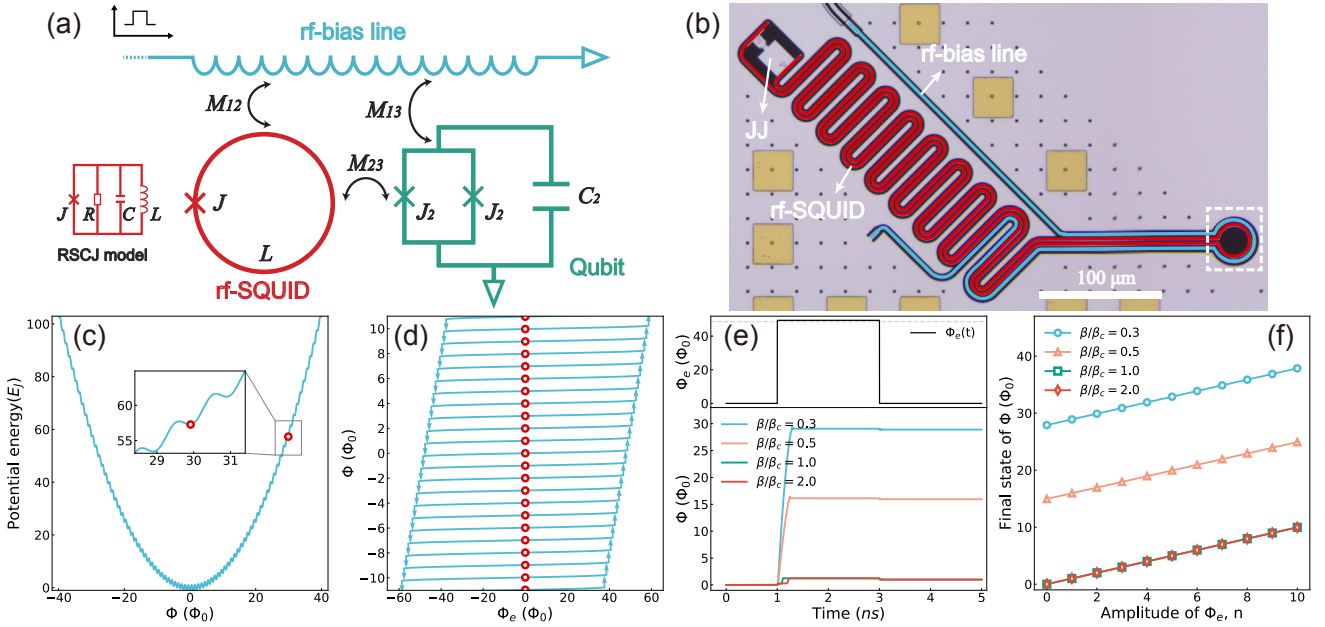


FIG. 1. Tuning qubit frequency by rf-SQUID. (a) Schematic circuit diagram of tuning the transition frequency of transmon by an rf-SQUID. (b) Optical micrograph of the rf-SQUID on the bottom chip of our flip-chip sample. The red line represents the inductance loop of rf-SQUID which is connected by a JJ and the blue line outlines rf-bias line. The white dashed square represents the area where the rf-SQUID and the rf-bias line interact with qubit (not shown) via spatial inductive coupling. (c) A numerical example of the potential energy curve of the rf-SQUID when external magnetic flux $\Phi_e = 0$ for $I_c = 100 \mu\text{A}$, $L = 1 \text{ nH}$, and $\beta_e = 303.9$. The horizontal axis is the total magnetic flux Φ of rf-SQUID and the vertical axis represents the potential energy U in the unit of Josephson energy $E_J = I_c \Phi_0 / 2\pi$. The inset figure shows the detail of the local tilted washboard potential well located at $\Phi \approx 30 \Phi_0$. (d) A numerical example of hysteresis curve between external magnetic flux Φ_e and total magnetic flux Φ of rf-SQUID with the same parameters settings in (c). The red circles indicate the position of local metastable states for $\Phi_e = 0$ which are consistent with those shown in (c). (e) A numerical example of modulating the state of rf-SQUID by inputting a single pulsed signal for different damping condition. The parameters in simulation are chosen $I_c = 100 \mu\text{A}$, $L = 1 \text{ nH}$, $C = 2 \text{ pF}$ and $R = 3.6 \Omega$, 2.2Ω , 1.1Ω , 0.5Ω for $\beta/\beta_c = 0.3$, 0.5 , 1.0 , 2.0 , respectively. The initial state of rf-SQUID is set to $\Phi = 0$. The amplitude of the pulse is chosen as $\Phi_e = (\beta_e/2\pi + 1)\Phi_0 = 49.4\Phi_0$ and the critical value of Φ_e when $\Phi = 0$ is $\Phi_{e,c} = (\beta_e/2\pi + 1/4)\Phi_0 = 48.6\Phi_0$, which is shown by the light grey dashed line in the upper subfigure. (f) A numerical example of the linear relationship of magnetic flux transition of rf-SQUID for different damping conditions with the same simulation parameters settings in (e). The horizontal axis represents the amplitude of the pulse in simulation $\Phi_e = [\beta_e/(2\pi) + n]\Phi_0$ with $n = 0, 1, \dots, 10$. The result of $\beta/\beta_c = 1.0$ coincides with that of $\beta/\beta_c = 2.0$. All results share a same slope $k = 1$.

($n_i - 1 - (\beta_e/2\pi + 1/4), n_i - (\beta_e/2\pi + 1/4)$), rf-SQUID will evolve into a temporal position $\Phi_r \approx n_r \Phi_0$ which satisfies $|\Phi_r - \Phi_i| = \Delta\Phi$. Secondly, another input single pulse with positive amplitude $\Phi_{e,2}/\Phi_0 \in [n_r + n_f - n_i + (\beta_e/2\pi + 1/4), n_r + n_f - n_i + 1 + (\beta_e/2\pi + 1/4)]$ (deduced from the linear magnetic flux transition relationship) will modulate rf-SQUID to the target state Φ_f . There are similar strategies for $n_f < n_i$ cases.

DESIGN AND EXPERIMENT

Fig. 1(b) shows an optical micrograph of the rf-SQUID of our sample, where the red line represents the inductance loop of rf-SQUID which is connected by a JJ and the blue line outlines the rf-bias line. The chip has a flip-chip structure which is fabricated by the micro-nano fabrication technology developed in our *Zuchongzhi* se-

ries quantum processor [2].

TABLE I. Parameters of rf-SQUID

Parameters	Value
Josephson current I_c	$320 \mu\text{A}$
Self-inductance L	1.18 nH
Mutual inductance M_{12}	70 pH
Mutual inductance M_{13}	2.90 pH
Mutual inductance M_{23}	4.07 pH

In the experiment, we firstly use the rf-bias line as XY-drive line and Z-control line to calibrate qubits after the chip installed into a dilute refrigerator reaching temperature below 20 mK. After calibrating basic qubit properties, we input single square wave voltage signal from room-temperature electronics into the rf-bias line to modulate the state of rf-SQUID. The pulsed signal typically has an amplitude of 7 V and a duration of 100

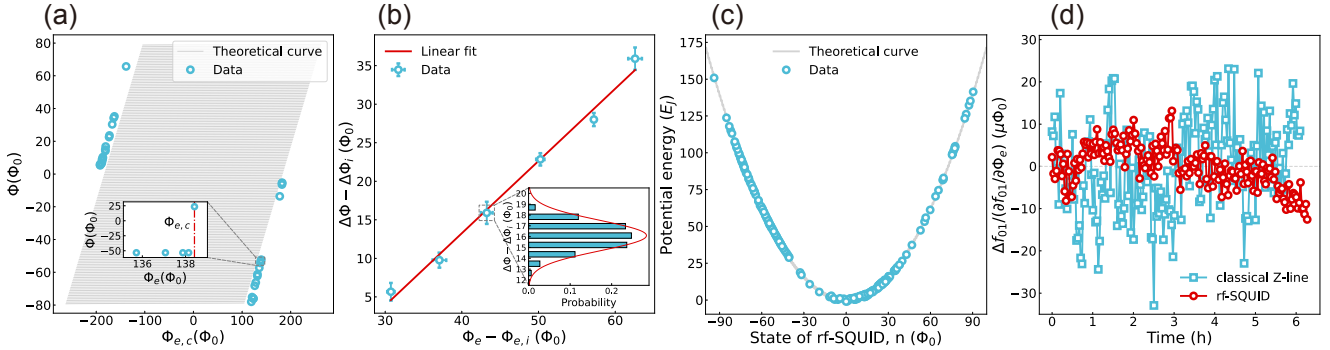


FIG. 2. Experimental results of modulating rf-SQUID states by single square wave pulses. (a) The hysteresis result between critical external magnetic flux $\Phi_{e,c}$ and states Φ of rf-SQUID. The experimental data is shown in blue circles and the theoretical curve is shown in light grey lines. The inset figure shows an example that rf-SQUID does not change from the initial position $-53.2 \Phi_0$ to the final position $23.5 \Phi_0$ until the amplitude of the pulse reaches its critical value $\Phi_{e,c} = 138.4 \Phi_0$. (b) The result of magnetic flux transition experiment. We repeatedly prepare the initial state $\Phi_i = (-57.5 \pm 1) \Phi_0$ for rf-SQUID, whose critical amplitude of the pulse is $\Phi_{e,i} = (94.9 \pm 1) \Phi_0$. We vary the amplitude Φ_e and collect the final state Φ_f of rf-SQUID. The horizontal axis represents the difference between the amplitude Φ_e of input pulse and the critical amplitude $\Phi_{e,i} = (94.9 \pm 1) \Phi_0$ of the pulse of the initial state. The vertical axis represents the difference $\Delta\Phi - \Delta\Phi_i$ of the magnetic flux transition, where $\Delta\Phi = \Phi_f - \Phi_i$, $\Delta\Phi_i = \Phi_{f,i} - \Phi_i = 76.7 \Phi_0$ and $\Phi_{f,i}$ represents the final state of rf-SQUID when inputting pulse with critical amplitude $\Phi_{e,i}$. Each data (blue circle) is sampled for at least 4 times. The linear fit result $\Delta\Phi - \Delta\Phi_i = k(\Phi_e - \Phi_{e,i}) + b$ with $k = 0.94(0.05)$ and $b = -24.23(2.17)$ demonstrates that the data aligns well with theoretical linear trend. The inset figure shows the detailed distribution of the magnetic flux transition at the 3rd data point. The result contains 626 data and is fit by Gaussian function $p = 1/(\sqrt{2\pi}\sigma)e^{-(x-x_0)/2\sigma^2}$ with $x_0 = 16.1(0.1)$ and $\sigma = 1.4(0.1)$. (c) The statistics of the local potential wells of rf-SQUID by varying the amplitude of single square wave pulse in the experiment. The horizontal axis represents the state n of rf-SQUID, and the vertical axis represents the potential energy in the unit of Josephson energy E_J . The result contains total 171 data (blue circles). (d) Comparison of the stability results of qubit frequency f_{01} collected under rf-SQUID scheme and classical Z-line scheme, respectively. The red circles represent the data collected under rf-SQUID scheme with $f_{01} = 4.5904$ GHz whose maximum f_{01} is 5.1387 GHz. The blue squares are the data collected under the classical Z-line scheme with $f_{01} = 4.4727$ GHz whose maximum f_{01} is 5.0069 GHz. Each data point is sampled for every 2 minutes. The y-axis represents the relative qubit frequency Δf_{01} difference from the mean f_{01} , divided by the derivative of f_{01} versus external magnetic flux Φ_e for qubit. The peak-to-peak (P2P) value and standard deviation (STD) of f_{01} for rf-SQUID case are P2P = $25.7 \mu\Phi_0$ and STD = $4.9 \mu\Phi_0$, while for the classical Z-line case, these results are P2P = $56.0 \mu\Phi_0$ and STD = $11.0 \mu\Phi_0$.

ns, which goes through total 34 dB attenuators along coaxial cables in the dilute refrigerator. After modulation, no more signal to tune qubit frequency is input and we deduce the state information of rf-SQUID from qubit frequency calibrated by Ramsey experiment.

Table I lists the parameters of the rf-SQUID in the experiment. These parameters enable total $2 \times \lfloor \beta_e/2\pi + 1/4 \rfloor - 1 = 363$ local potential wells and maximum magnetic flux $0.63 \Phi_0$ provided for qubit. The difference in the magnetic flux between the adjacent wells of rf-SQUID approximates $1 \Phi_0$, thus the magnetic flux step providing for qubit is $0.0034 \Phi_0$ under these parameters, which is sufficient for traversing qubit frequencies. Moreover, combining the data from current-voltage (I-V) curve of the JJ in rf-SQUID, the damping condition of rf-SQUID satisfies $\beta = 12.1 < \beta_c = 40.1$, which indicates the underdamped condition of rf-SQUID [22].

Since the rf-SQUID is underdamped, we scan the hysteresis curve by alternately modulating the state Φ of rf-SQUID back and forth between positive and negative positions, which is achieved by inputting corresponding single pulses with negative and positive amplitudes. Fig.

2(a) shows the experimental result. Here the vertical axis is the state Φ of rf-SQUID deduced from qubit frequency. The horizontal axis represents the critical amplitude $\Phi_{e,c}$ of the pulse which begins to modulate rf-SQUID. And the inset figure exhibits an example that rf-SQUID does not change from the initial position $-53.2 \Phi_0$ to the final position $23.5 \Phi_0$ until the amplitude of the pulse reaches its critical value $138.4 \Phi_0$.

We then perform the linear magnetic flux transition experiment with the initial state of rf-SQUID repeatedly prepared to the target position $\Phi_i = (-57.5 \pm 1) \Phi_0$. After preparation, we vary the amplitudes of single square wave voltage pulses to investigate the magnetic flux transition relation. In the experiment, the positive critical amplitude of Φ_i is $\Phi_{e,i} = (94.9 \pm 1) \Phi_0$ which is different from the theoretical prediction $\Phi_{e,i,predict} = (125.4 \pm 1) \Phi_0$. We attribute this difference to the environmental magnetic flux around rf-SQUID when we perform the experiment [22]. Fig. 2(b) shows both the experimental result and the linear fit result of the data which is in good agreement with theoretical linear trend shown in Fig. 1(f). We also find that the y-intercept of linear fit

result $b = -24.23(2.17)$ shifts away from 0. We attribute this difference to the additional insertion loss along coaxial cables in dilute refrigerator and the distortion of the rising edge of the voltage pulse, which makes the actual amplitude of the pulse input into rf-bias line smaller than the set value in practice. These factors indicate that it's preferable to precompensate an additional increase in the amplitude so as to refer to the linear response relationship between Φ and Φ_e to modulate rf-SQUID to a specific state. In our system, the precompensation of the additional increase of Φ_e should be at least $24 \Phi_0$. The inset figure in Fig. 2(b) shows the detailed distribution of the magnetic flux transition at the 3rd data point which is well fit by Gaussian function.

By combining the results in Fig. 2(a,b) and varying the amplitude of input pulse, we collect total 171 local potential wells of rf-SQUID in the experiment which is shown in Fig. 2(c). This result indicates that the rf-SQUID provides qubit with maximum magnetic flux $0.32 \Phi_0$, which tunes qubit frequency from maximum 5.1387 GHz to minimum 3.7721 GHz.

In addition, we compare the stability of qubit frequency obtained under the rf-SQUID scheme and the classical Z-line scheme, respectively. As shown in Fig. 2(d), the fluctuation in unit of magnetic flux under rf-SQUID scheme with peak-to-peak value of $P2P = 25.7 \mu\Phi_0$ and standard deviation of $STD = 4.9 \mu\Phi_0$, is less than that of the classical Z-line scheme with $P2P = 56.0 \mu\Phi_0$ and $STD = 11.0 \mu\Phi_0$. This result indicates that the magnetic flux provided by *in situ* rf-SQUID with RSD 24.5 PPM is more stable than the magnetic flux provided by the current in Z-line input from room-temperature electronics(driven by 16-bit resolution digital-to-analog converter[2]), whose RSD is 55.0 PPM. For the non-zero fluctuation of magnetic flux under the rf-SQUID scheme, the main reason is the connection between the rf-bias line and the room-temperature electronics resource, which transports the voltage fluctuation from room-temperature electronics to the rf-bias line [22].

CONCLUSION AND OUTLOOK

In this paper, we propose a low-power, scalable scheme to tune the transition frequency of superconducting qubit by using *in situ* rf-SQUID. With several single square wave pulses input, the superconducting current in rf-SQUID will be modulated and kept at the changed position indefinitely, providing qubit with almost constant magnetic flux. For critical damped and overdamped condition, one single pulse input is enough to modulate rf-SQUID to a specific state in principle. For underdamped condition, there are still some strategies to modulate rf-SQUID to a specific position with several single pulses input. We design and fabricate a sample to investigate the properties of the underdamped rf-SQUID. The ex-

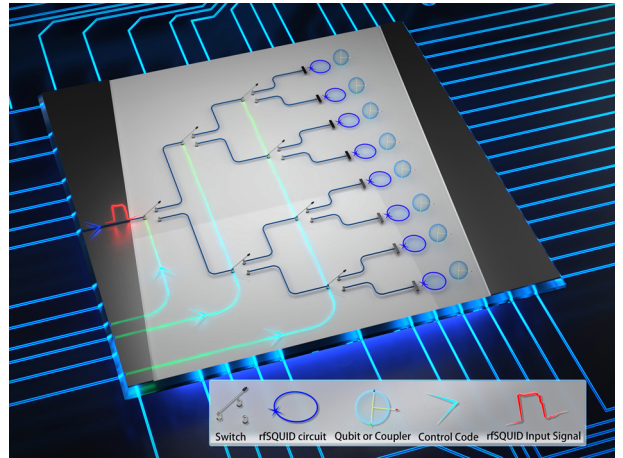


FIG. 3. A time-division-multiplex (TDM) scheme of controlling qubit frequencies by combining rf-SQUID with on-chip single-pole double-throw switch arrays [25, 26], which paves the way to scalable superconducting quantum processor. With the help of switch array, the number of cables for transmitting the pulsed signal for rf-SQUID could be reduced. For instance, a two-dimensional square lattice quantum processor with n qubits and $\sim 2n$ couplers connecting nearest neighboring qubits needs $\sim 3n$ Z-line cables in usual scheme. In contrast, the number of cables could be reduced to $\sim \log_2(3n) + 1$ with the combination of rf-SQUID and switch arrays. To be specific, only one cable and one channel signal source in room temperature are required in principle to transmit the pulsed signal for rf-SQUID, which could significantly reduce the power consumption compared with the classical room-temperature electronics scheme, and the left $\sim \log_2(3n)$ cables are used for transmitting the control code to address rf-SQUIDs i.e., qubits or couplers. And it's straightforward to find a truth table for the control code to determine which rf-SQUID to modulate.

perimental results match well with the theoretical prediction, enabling us to modulate rf-SQUID from an initial state to a specific state by inputting several single square wave pulses. In addition, we also find that the stability of qubit frequency under rf-SQUID scheme is better than that of the classical Z-line scheme. Besides the application for transmon qubit mentioned above, our scheme shall be applied for any other type of qubit whose frequency could be modified by constant magnetic flux. In the very near future, a shunted resistance along the JJ in the rf-SQUID is going to be fabricated to make rf-SQUID reach overdamped condition, which will simplify the pulse inputting strategy. Moreover, by combining the rf-SQUID with switch arrays as shown in Fig 3, the number of cables in dilute refrigerator for Z-control could be reduced from usual $\sim 3n$ to $\sim \log_2(3n) + 1$ and only one room-temperature electronics for modulating rf-SQUID is needed in principle, which could significantly reduce the power consumption, thus paving the way to low-power and scalable control of large-scale superconducting processors.

The authors thank the USTC Center for Micro- and Nanoscale Research and Fabrication for supporting the sample fabrication and QuantumCTek Co., Ltd. for supporting the fabrication and maintenance of room-temperature electronics. This research was supported by the Innovation Program for Quantum Science and Technology (Grant No. 2021ZD0300200), Shanghai Municipal Science and Technology Major Project (Grant No. 2019SHZDZX01), Anhui Initiative in Quantum Information Technologies, the New Cornerstone Science Foundation through the XPLORER PRIZE, the Key-Area Research and Development Program of Guangdong Province (Grant No. 2020B0303060001), Special funds from Jinan science and Technology Bureau and Jinan high tech Zone Management Committee. Y.X. acknowledges support from the Shanghai Sailing Program.

* These authors contributed equally to this work.

† Present address: RIKEN Center for Quantum Computing (RQC), Wako, Saitama 351-0198, Japan

‡ jinjinli@nim.ac.cn

§ xbzhu16@ustc.edu.cn

¶ pan@ustc.edu.cn

- [1] F. Arute, K. Arya, R. Babbush, D. Bacon, J. C. Bardin, R. Barends, R. Biswas, S. Boixo, F. G. Brandao, D. A. Buell, *et al.*, Quantum supremacy using a programmable superconducting processor, *Nature* **574**, 505 (2019).
- [2] Y. Wu, W.-S. Bao, S. Cao, F. Chen, M.-C. Chen, X. Chen, T.-H. Chung, H. Deng, Y. Du, D. Fan, *et al.*, Strong quantum computational advantage using a superconducting quantum processor, *Physical review letters* **127**, 180501 (2021).
- [3] Q. Zhu, S. Cao, F. Chen, M.-C. Chen, X. Chen, T.-H. Chung, H. Deng, Y. Du, D. Fan, M. Gong, *et al.*, Quantum computational advantage via 60-qubit 24-cycle random circuit sampling, *Science bulletin* **67**, 240 (2022).
- [4] A. Morvan, B. Villalonga, X. Mi, S. Mandra, A. Bengtsson, P. Klimov, Z. Chen, S. Hong, C. Erickson, I. Drozdov, *et al.*, Phase transition in random circuit sampling, *arXiv preprint arXiv:2304.11119* (2023).
- [5] R. Barends, J. Kelly, A. Megrant, A. Veitia, D. Sank, E. Jeffrey, T. C. White, J. Mutus, A. G. Fowler, B. Campbell, *et al.*, Superconducting quantum circuits at the surface code threshold for fault tolerance, *Nature* **508**, 500 (2014).
- [6] F. Yan, P. Krantz, Y. Sung, M. Kjaergaard, D. L. Campbell, T. P. Orlando, S. Gustavsson, and W. D. Oliver, Tunable coupling scheme for implementing high-fidelity two-qubit gates, *Physical Review Applied* **10**, 054062 (2018).
- [7] R. Barends, C. Quintana, A. Petukhov, Y. Chen, D. Kafri, K. Kechedzhi, R. Collins, O. Naaman, S. Boixo, F. Arute, *et al.*, Diabatic gates for frequency-tunable superconducting qubits, *Physical review letters* **123**, 210501 (2019).
- [8] M. McEwen, D. Kafri, Z. Chen, J. Atalaya, K. Satzinger, C. Quintana, P. V. Klimov, D. Sank, C. Gidney, A. Fowler, *et al.*, Removing leakage-induced correlated errors in superconducting quantum error correction, *Nature communications* **12**, 1761 (2021).
- [9] R. Bialczak, M. Ansmann, M. Hofheinz, M. Lenander, E. Lucero, M. Neeley, A. O’Connell, D. Sank, H. Wang, M. Weides, *et al.*, Fast tunable coupler for superconducting qubits, *Physical review letters* **106**, 060501 (2011).
- [10] J. Clarke, Advances in squid magnetometers, *IEEE Transactions on Electron Devices* **27**, 1896 (1980).
- [11] J. Clarke and A. I. Braginski, *The SQUID handbook*, Vol. 1 (Wiley Online Library, 2004).
- [12] H. Smith and J. A. Blackburn, Multiple quantum flux penetration in superconducting loops, *Physical Review B* **12**, 940 (1975).
- [13] J. A. Blackburn and H. Smith, Multiple-quantum-flux penetration in a superconducting loop containing a josephson junction: Temperature dependence, *Physical Review B* **35**, 1659 (1987).
- [14] R. L. Peterson and R. I. Gayley, Multiple magnetic flux entry into superconducting quantum-interference devices (squids): A general way of examining the $\cos \varphi$ conductance, *Physical Review B* **18**, 1198 (1978).
- [15] J. R. Friedman, V. Patel, W. Chen, S. Tolpygo, and J. E. Lukens, Quantum superposition of distinct macroscopic states, *nature* **406**, 43 (2000).
- [16] R. McDermott, R. Simmonds, M. Steffen, K. B. Cooper, K. Cicak, K. Osborn, S. Oh, D. P. Pappas, and J. M. Martinis, Simultaneous state measurement of coupled josephson phase qubits, *Science* **307**, 1299 (2005).
- [17] M. W. Johnson, M. H. Amin, S. Gildert, T. Lanting, F. Hamze, N. Dickson, R. Harris, A. J. Berkley, J. Johansson, P. Bunyk, *et al.*, Quantum annealing with manufactured spins, *Nature* **473**, 194 (2011).
- [18] A. Lupaşcu, C. Verwijs, R. Schouten, C. Harmans, and J. Mooij, Nondestructive readout for a superconducting flux qubit, *Physical review letters* **93**, 177006 (2004).
- [19] K. Cooper, M. Steffen, R. McDermott, R. W. Simmonds, S. Oh, D. A. Hite, D. P. Pappas, and J. M. Martinis, Observation of quantum oscillations between a josephson phase qubit and a microscopic resonator using fast readout, *Physical Review Letters* **93**, 180401 (2004).
- [20] M. S. Allman, F. Altomare, J. D. Whittaker, K. Cicak, D. Li, A. Sirois, J. Strong, J. D. Teufel, and R. W. Simmonds, rf-squid-mediated coherent tunable coupling between a superconducting phase qubit and a lumped-element resonator, *Physical review letters* **104**, 177004 (2010).
- [21] P. Krantz, M. Kjaergaard, F. Yan, T. P. Orlando, S. Gustavsson, and W. D. Oliver, A quantum engineer’s guide to superconducting qubits, *Applied physics reviews* **6** (2019).
- [22] See supplementary material (2024).
- [23] A. Barone and G. Paterno, *Physics and applications of the Josephson effect*, Vol. 1 (Wiley Online Library, 1982).
- [24] K. K. Likharev, *Dynamics of Josephson junctions and circuits* (Routledge, 2022).
- [25] M. Pechal, J.-C. Besse, M. Mondal, M. Oppiger, S. Gasparinetti, and A. Wallraff, Superconducting switch for fast on-chip routing of quantum microwave fields, *Phys. Rev. Appl.* **6**, 024009 (2016).
- [26] J. Zotova, A. Semenov, R. Wang, Y. Zhou, O. Astafiev, and J.-S. Tsai, Tunable compact on-chip superconducting switch, *Phys. Rev. Appl.* **21**, 024059 (2024).
- [27] M. Tinkham, *Introduction to superconductivity* (Courier Corporation, 2004).

[28] K. Likharev, Superconducting weak links, *Reviews of Modern Physics* **51**, 101 (1979).

[29] R. F. Voss and R. A. Webb, Macroscopic quantum tunneling in 1- μ m nb josephson junctions, *Phys. Rev. Lett.* **47**, 265 (1981).

**Supplemental Material for
“*In situ* Qubit Frequency Tuning Circuit for Scalable Superconducting Quantum Computing: Scheme and Experiment”**

UNDERDAMPED CONDITION

In this section, we calculate the damping condition of the rf-SQUID. The experimental I-V data in Fig. S1 shows that the Josephson critical current is $I_c = 320 \mu A$, the retrapping current is $I_r = 146 \mu A$ and the slope by linear fitting the R branch is $R = 1.85 \Omega$. According to these values, we could get the shunted capacitance $C = 2.34 \text{ pF}$, the parameter $\beta = 1/R\sqrt{L/C} = 12.1$, and the critical quality factor $\beta_c = 40.1$ [27, 28]. Since $\beta = 12.1 < \beta_c = 40.1$, the rf-SQUID is underdamped.

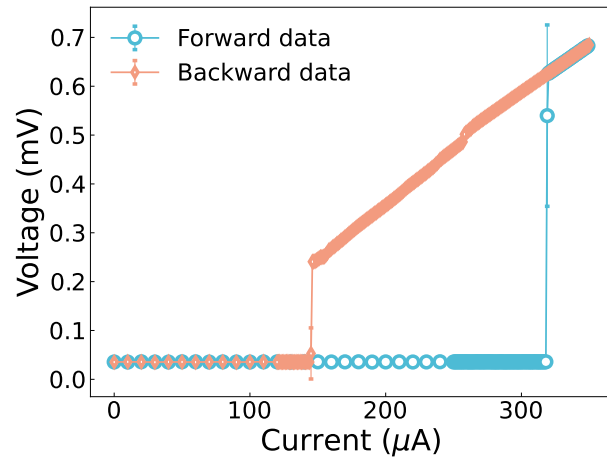


FIG. S1. The I-V curve of a JJ on the bottom chip, which is fabricated simultaneously with the JJ in rf-SQUID with the same fabrication parameters. The blue circles present the data obtained while increasing the current from 0 to $350 \mu A$, while the orange diamonds present the data while decreasing the current from $350 \mu A$ to 0. The Josephson critical current is $I_c = 320 \mu A$, the retrapping current is $I_r = 146 \mu A$ and the slope of the R branch by linear fitting is $R = 1.85 \Omega$.

THERMAL EXCITATION RATE

The lifetime of the state of rf-SQUID could be affected by the thermal excitation rate. According to ref [29], the thermal excitation rate is

$$\Gamma = \frac{\omega_{p,i}}{2\pi} \cdot e^{-\frac{H(i)}{k_B T}} \quad (\text{S1})$$

where $\omega_{p,i} = \omega_{p,0}(1 - i^2)^{1/4}$, $\omega_{p,0} = \sqrt{\frac{2\pi I_c}{\Phi_0 C}}$, $i = I/I_c$, $H(i) = \frac{I_c \Phi_0}{\pi} (\sqrt{1 - i^2} - i \arccos i) - \frac{\hbar \omega_{p,i}}{2}$ and I presents the current in rf-SQUID. Using the data from above section, we could calculate that the thermal excitation rate reaches a maximum value of $\Gamma_{max} = 3.68 \times 10^{-285}$ when rf-SQUID lies at the maximum position $\Phi_{max} \approx 180.8\Phi_0$, which indicates that the lifetime of the metastable state of rf-SQUID is nearly infinite at the typical temperature of 20mK. Even the environmental temperature rises up to 100mK, the maximum thermal excitation rate reaches $\Gamma_{max} = 3.82 \times 10^{-49}$, which is still low enough. The low thermal excitation rate shall be attributed to the high plasma frequency $\omega_{p,0} = 2\pi \times 102.6 \text{ GHz}$ of rf-SQUID, which indicates that the local potential well is quite deep.

INFLUENCE OF ENVIRONMENTAL MAGNETIC FLUX

The hysteresis relationship between total magnetic flux Φ of the rf-SQUID and the external magnetic flux Φ_e could be affected by the constant environmental magnetic flux. Fig. S2 shows an example of the hysteresis curves deviated by the constant environmental magnetic flux. The existence of the environmental magnetic flux shall affect the magnetic flux threshold i.e., the voltage amplitude in experiment when modulating rf-SQUID. Thanks to the truth that the environmental magnetic flux is often constant in practice, the influence of the environmental magnetic flux is limited. There is around $30.5 \Phi_0$ environmental magnetic flux in the linear magnetic flux transition experiment of the main text.

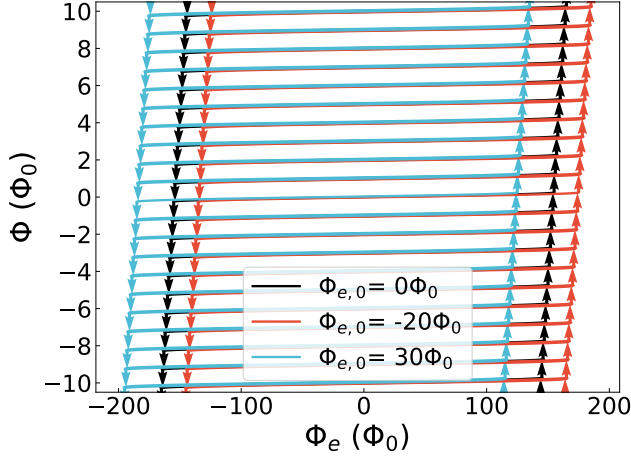


FIG. S2. Hysteresis curves affected by different constant environmental magnetic flux. Here the environmental magnetic flux $\Phi_{e,0}$ are set to 0, -20, 30 Φ_0 with $I_c = 100 \mu A$, $L = 1 nH$, $\beta_e = 303.9$.

FLUCTUATION OF VOLTAGE OUTPUT FROM ROOM-TEMPERATURE ELECTRONICS

For rf-SQUID scheme, there is still non-zero fluctuation of qubit frequency in the main text. The main reason is the connection between the on-chip rf-bias line and the room-temperature electronics resource in experiment, which shall transport the voltage fluctuation from room-temperature electronics to the rf-bias line. A typical result of voltage fluctuation from room-temperature electronics is shown in Fig. S3. When the voltage output approaches zero i.e., -3.256 mV, the fluctuation in voltage with P2P = 0.012 mV will cause fluctuation in magnetic flux for qubit with P2P = 15.3 $\mu\Phi_0$. When electronics resource outputs voltage 188.797 mV, which changes f_{01} from maximum 5.0069 GHz to 4.4727 GHz in the main text, the fluctuation in voltage increases to P2P = 0.036 mV which will cause the fluctuation in magnetic flux for qubit with P2P = 50.2 $\mu\Phi_0$.

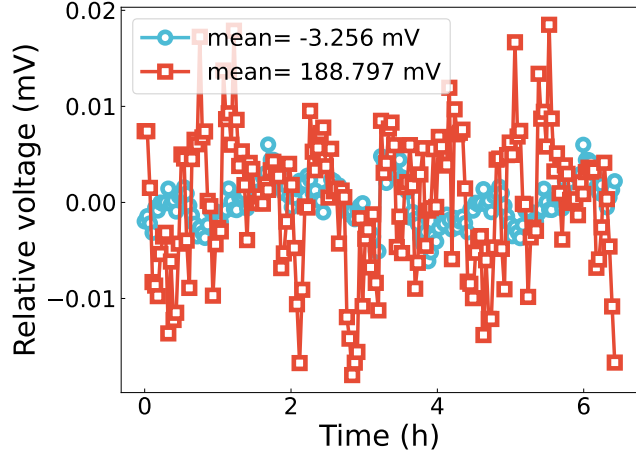


FIG. S3. A typical voltage fluctuation of room-temperature electronics resource. The vertical axis presents the relative voltage difference from the mean voltage. The blue circles present the data with mean voltage -3.256 mV, whose peak-to-peak(P2P) value is 0.012 mV. The red squares present the data with mean voltage 188.797 mV, whose P2P is 0.036 mV. Each data is averaged within 1 minute and the time interval is 2 minutes.